Processing and Application of Ceramics 13 [3] (2019) 269–276
https://doi.org/10.2298/PAC1903269S

Comparison between dielectric and pyroelectric properties of PZFNT and BST type ceramics

Viorica Stancu, Luminita Amarande, Mihaela Botea, Alin Iuga, Lucia N. Leonat, Aandrei G. Tomulescu, Marius Cioangher, Luminita M. Balescu, Lucian Pintilie*

National Institute of Materials Physics, Atomistilor Str., No. 405A, 077125, Magurele-Ilfov, Romania

Received 11 April 2019; Received in revised form 17 July 2019; Accepted 5 August 2019

Abstract

$Ba_{0.75}Sr_{0.25}TiO_3$ (BST) and $PbZr_{0.68}Fe_{0.14}Nb_{0.14}Ti_{0.04}O_3$ (PZFNT) ceramic pellets were obtained by ceramic technology and their structural, ferroelectric and pyroelectric properties were investigated. The relative density of BST and PZFNT is about 93% and 90%, respectively, with an average grain size of 102 μm and 6.45 μm. Both materials have similar room temperature dielectric constants (~2000), but PZFNT shows higher remnant polarization (~15 μC/cm^2) and better pyroelectric properties (~ $1.69 \cdot 10^{-4}$ C/m^{2}K), which recommend it for pyroelectric detectors, infrared radiation- and laser pulse energy-meters.

Keywords: *BST, PZFNT, pyroelectric characterization*

I. Introduction

The interest for perovskite type oxide ceramics (ABO_3) such as lead zirconate titanate (PZT) or barium strontium titanate (BST) is increased due to their ferro-, piezo- and pyro-electric performances. These features endorse this type of materials for micro- and optoelectronic applications, such as non-volatile memories (FRAMs), waveguides, IR detectors, etc. There are many similarities, but also differences between BST and PZT materials. Both BST and PZT have a polymorphic transformation from cubic (*paraelectric*) to tetragonal (*ferroelectric*) phase, possessing the same type of perovskite structure [1], but BST has two more polymorphic transitions, at lower temperatures, between the ferroelectric phases. Moreover, these oxides have distinct macroscopic properties [2,3]: the transition temperature and remnant polarization are much higher for PZT compared to BST [4], while the dielectric constant is usually higher for BST [5]. The aim of this work was to investigate and compare the morpho-structural, dielectric, ferroelectric and pyroelectric properties [5–8] of very thin ceramic disc samples (250 μm thickness), with a large diameter of 30 mm, in respect with their possible applications in laser pulse energy measurement [9]. Such functionalities require samples with a very small thickness to reduce the thermal inertia of the detector, and large diameter to decrease the energy density of the laser beam on the detector surface, thus preventing its damaging. Such a large aspect ratio of the ceramic pellets rises several challenging issues during their processing and measurement, related to the presence of micro-cracks and pores that promote mechanical failure and dielectric breakdown. Two specific compositions were selected, namely $Ba_{0.75}Sr_{0.25}TiO_3$ (BST) and $PbZr_{0.68}Fe_{0.14}Nb_{0.14}Ti_{0.04}O_3$ (PZFNT), knowing that dopants in BST and PZT lead to lower transition temperatures, thus to larger values for the pyroelectric coefficient. One has also to mention that pyroelectric properties are usually investigated on samples of small area [10], and only few studies were performed on large area pyroelectric elements manufactured from ferroelectric polymers [11,12]. In the present study these properties are investigated on perovskite ceramic samples of large area, comparable to those used in commercial energy meters.

II. Experimental section

Lead zirconate titanate doped with iron and niobium ($PbZr_{0.68}Fe_{0.14}Nb_{0.14}Ti_{0.04}O_3$, PZFNT) and $Ba_{0.75}Sr_{0.25}TiO_3$ (BST) ceramics were prepared by the solid state synthesis method. The starting reagents for PZFNT were PbO (Merck, 99.7%), ZrO_2 (Fluka,

* Corresponding authors: tel: +40 723185411,
e-mail: *pintilie@infim.ro*

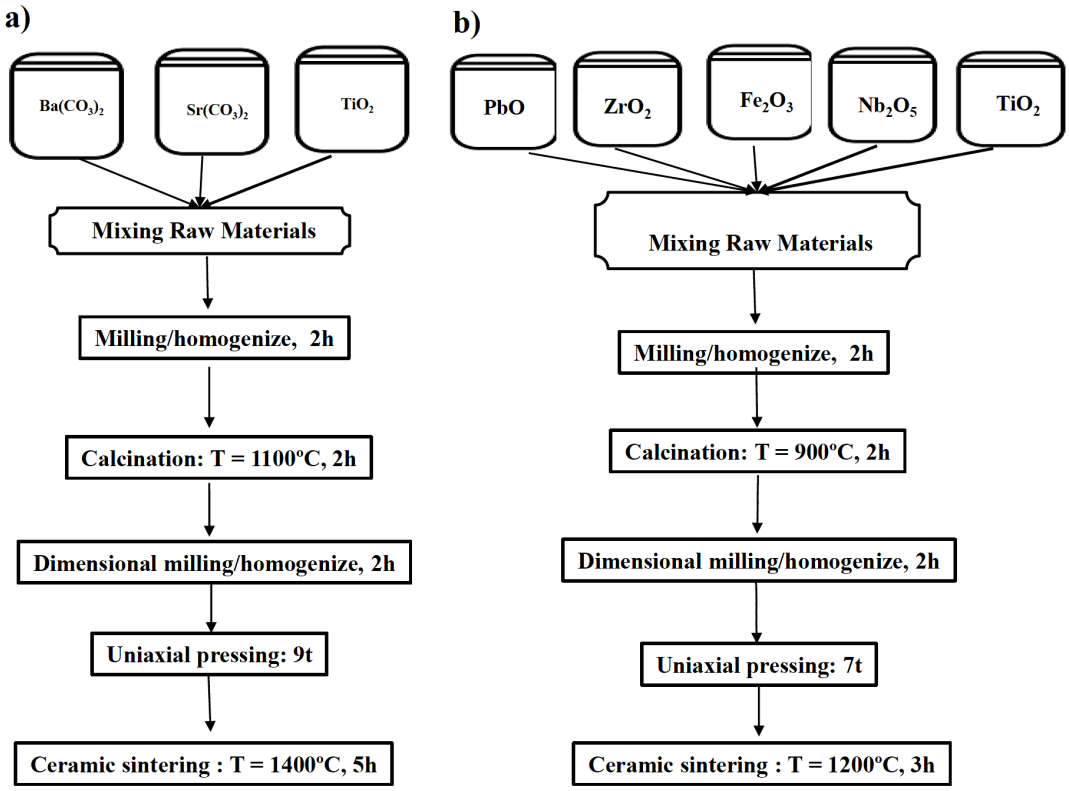

Figure 1. Flow diagram for the solid state processing of BST (a) and PZFNT (b) ceramics

99.8%), Nb_2O_5 (Fluka, 99.7%), iron trioxide Fe_2O_3 (Merck, 99.8%) and TiO_2 (Fluka, 99.5%). In the BST case, the raw materials were $Ba(CO_3)_2$, $Sr(CO_3)_2$ (Riedel de Haen, 99%) and TiO_2 (Fluka 99.8%) in stoichiometric ratios.

The starting oxide materials for both PZFNT and BST were mechanically mixed with ethanol (Chimopar, 99.6%), in a RETSCH planetary ball mill, for homogenization, at 300 rpm for 2 h. The resulting slurry was dried at 150 °C. The mixed powders were calcined at 900 °C for 2 h (PZFNT) and 1100 °C for 2 h (BST) and then milled again for 4 h in the planetary ball mill. Excess lead oxide of 1.5 mol% was added to the calcined powder of PZFNT before milling, to compensate for the lead loss during sintering and to improve ceramic densification by liquid phase formation.

The PZFNT and BST thin pellets with 30 mm diameter were obtained by cold uniaxial pressing with an equivalent force of 7 tones for PZT and 9 tones for BST. The compacted pellets were sintered at 1200 °C for 3 h (2 °C/min heating rate) in the case of PZFNT and 1400 °C for 5 h (3 °C/min heating rate) in the case of BST, resulting in the dense ceramic bodies. The bulk densities determined by the Archimedes' method were: 7.11 g/cm^3 for PZFNT and 5.59 g/cm^3 for BST. The flow diagram for the processing of these ceramics is presented in Fig. 1.

The morphology of PZFNT and BST ceramics was investigated with a Tescan Lyra 3XMU scanning electron microscope (SEM). The crystal structure was analysed by X-ray diffraction (XRD) using a Bruker D8 Advance equipment (powder setting). For electrical characterization, 200 μm Ni/Ag electrodes were deposited on both faces of PZFNT and BST thin ceramics (with thicknesses of 170 μm and 250 μm). The hysteresis measurements of the polarization versus the electric field were performed with a Precision LC II ferroelectric tester from Radiant Technologies Inc. The pyroelectric signal was recorded with a SR 830 DSP lock-in amplifier, using a J-FET type impedance converter. The IR source was a laser diode of 40 mW at 800 nm. The beam was modulated electronically using a signal generator from Tektronix, model AFG 3052C.

III. Results and discussion

The morphology of BST and PZFNT ceramics is illustrated in SEM images presented in Figs. 2a and 2b, respectively, showing a smooth, crack-free and dense structure with small pores between grains. The average grain size of 6.45 μm in PZFNT, and 102 μm in BST, can be correlated with the high sintering temperature of PZFNT and with the small strontium content of BST [10,11].

The crystallinity of PZFNT and BST ceramics was analysed by XRD measurements and indexed according to ASTM standards (Fig. 3). In both cases, a single phase structure was evidenced through sharp and intense peaks corresponding solely to the orthorhombic phase for PZNFT and the tetragonal phase for BST.

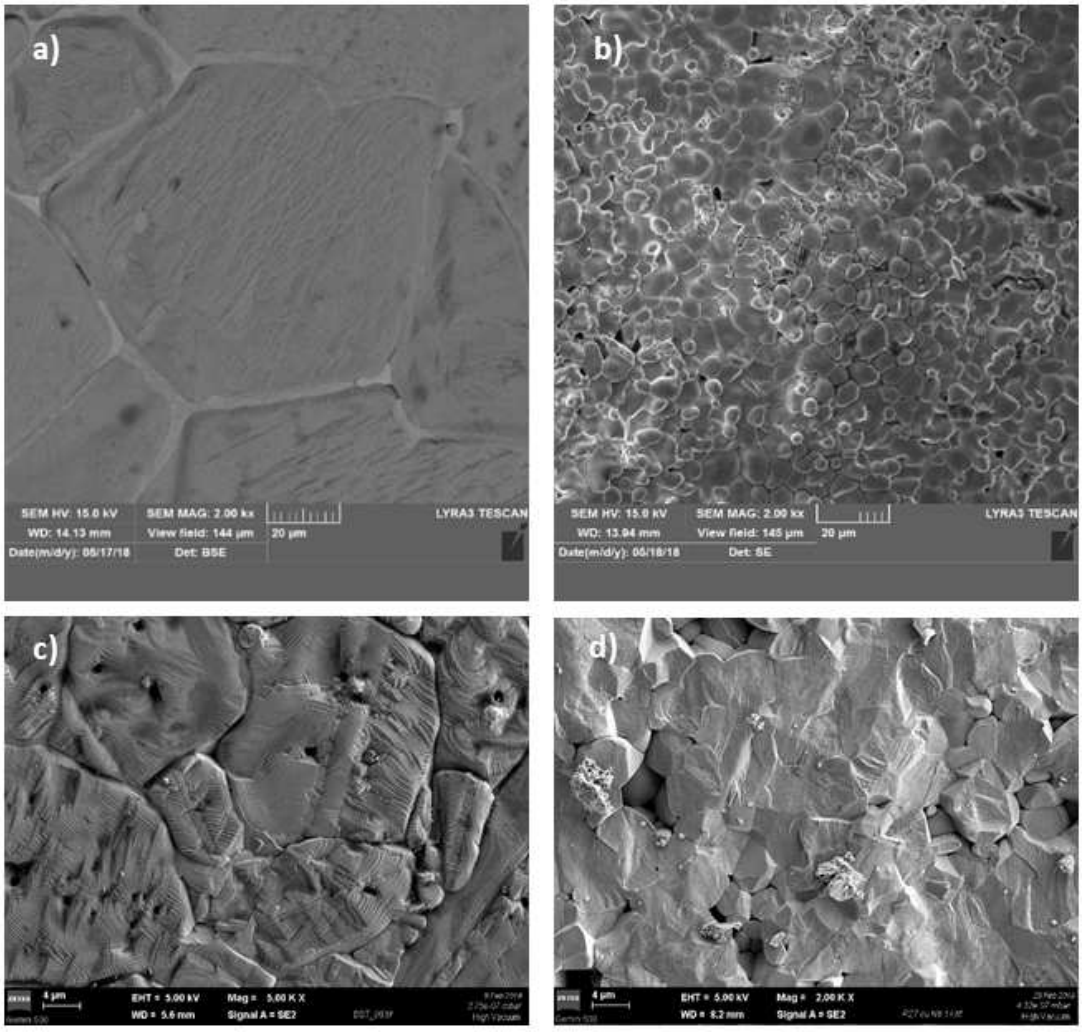

Figure 2. Surface morphology of BST (a) and PZFNT ceramics (b) and cross-section SEM image of BST (c) and PZFNT (d) ceramics

The ferroelectric properties of both materials were investigated by measuring the polarization P as a function of the applied electric field E. The resulting total, non-remnant and remnant hysteresis loops are depicted in Figs. 4a and 4b. The usually measured hysteresis loops represent the total polarization, including both remnant and non-remnant components. The non-remnant polarization reflects the contribution of the dielectric linear capacitance with losses, but also of the dipoles which are switched by the field and reverse after its removal.

The remnant polarization loop is given by the switched dipoles which preserve their orientation even

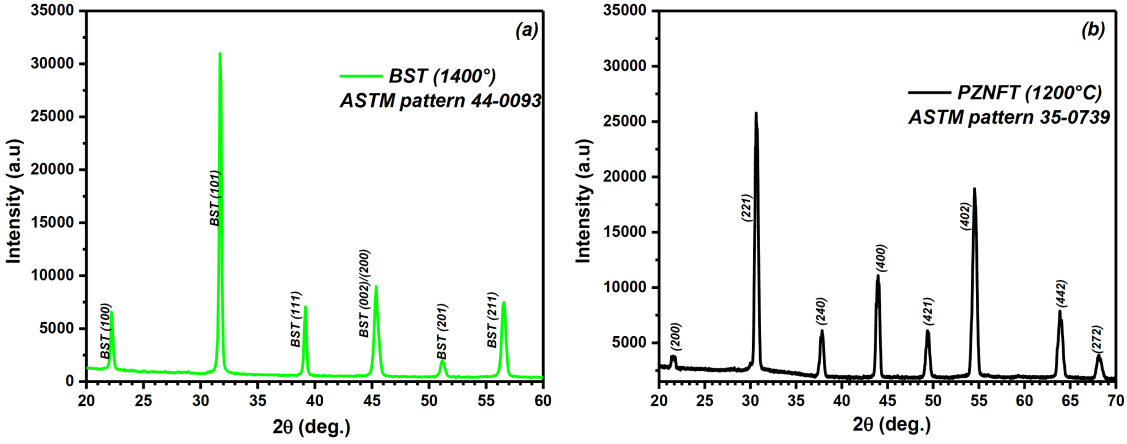

Figure 3. XRD pattern of: a) BST and b) PZFNT ceramics

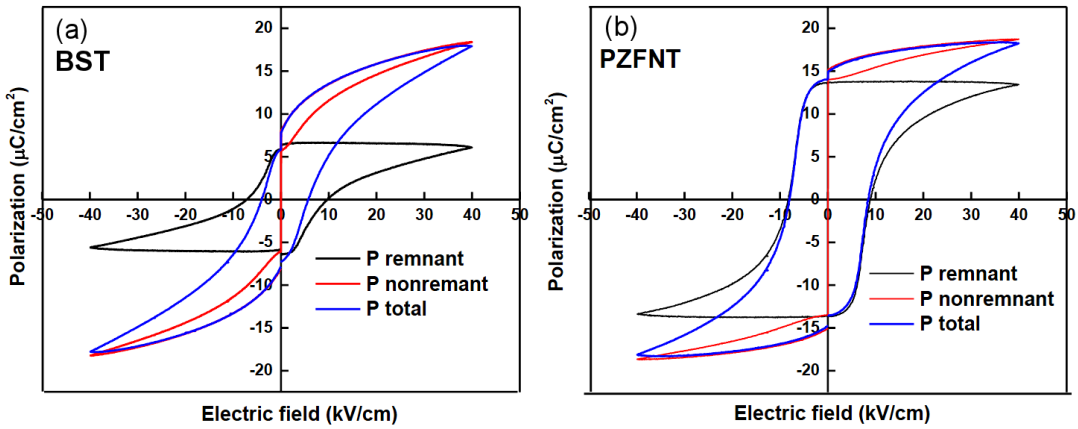

Figure 4. Polarization vs electric field hysteresis loops of: a) BST and b) PZFNT ceramics

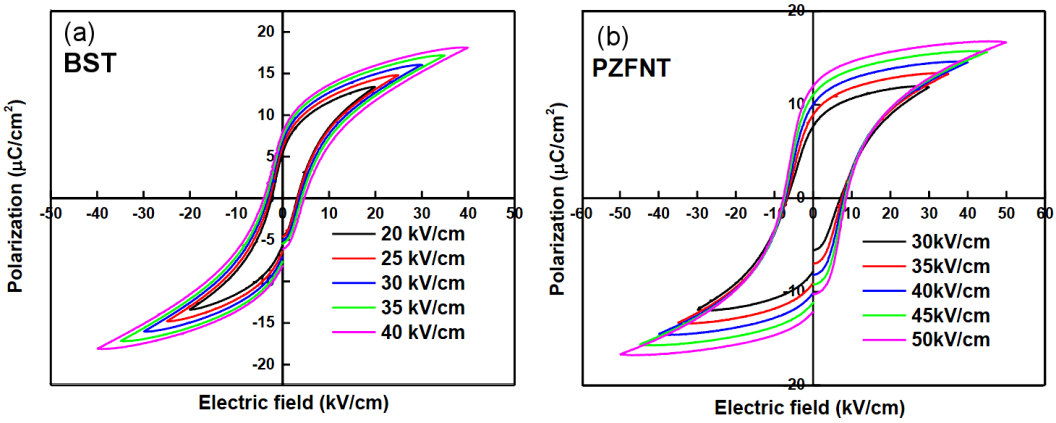

Figure 5. Evolution of *P-E* hysteresis loops with increasing the amplitude of the applied electric field on: a) BST and b) PZFNT ceramics

after the field was removed. This approach of ferroelectric characterization provides a more realistic evaluation of the ferroelectric versus dielectric response.

The hysteresis loops of these materials are quite different. The total polarization loop of BST is very slim, typical for a relaxor ceramics [12,13] compared to PZFNT loop, but shows a maximum polarization similar to that of PZFNT. The value of remnant polarization is the main difference between the hysteresis loops of these materials. BST has a remnant polarization of 6 μC/cm^2 representing half of the corresponding value of PZFNT. The coercive fields corresponding to remnant hysteresis loops have about the same values of 10 kV/cm for both materials, while the coercive field from the total polarization loop of BST is about 50% lower than for PZFNT due to the non-remnant response.

The hysteresis loops of the total polarization measured for different values (from 20 to 50 kV/cm) of the maximum electric field, are illustrated in Figs. 5a and 5b for BST and PZFNT, respectively.

As expected, the maximum polarization increases (with 40%) with increasing the intensity of the applied field, for both materials, without reaching saturation, while preserving the shape of the loops. Instead, the increase of the coercive field and remnant polarization is less evident, mostly for BST. The maximum electric field applied to BST was lower than for PZFNT because of its lower dielectric breakdown strength, possibly related to higher grain size effects [14,15].

Another interesting feature of the ferroelectric response is the effect of the polling process on the hysteresis loop of the total polarization, shown in Figs. 6a and 6b for BST and PZFNT, respectively. These figures display the hysteresis loops before (Fig. 6a) and after polling with 32 kV/cm for BST and 44 kV/cm for PZT, at room temperature for 15 min (Fig. 6b). The loops registered before and after polling were identical for BST, but quite different for PZT. Thus, the maximum and remnant polarization of PZFNT increased with 32% and 64% after polling, as a result of the enhanced domain wall mobility and redistribution of the space charge during polling with long lasting applied field compared to the hysteresis loop measurement. Despite the shift of the hysteresis loop on the horizontal axis, expected to occur after polling, assigned to the internal field and resulting from the dipole alignment, this was not experimentally observed in either of the two materials. This is the consequence of a very low remnant polarization of BST and of a small coercive field of PZFNT compared to the maximum applied field.

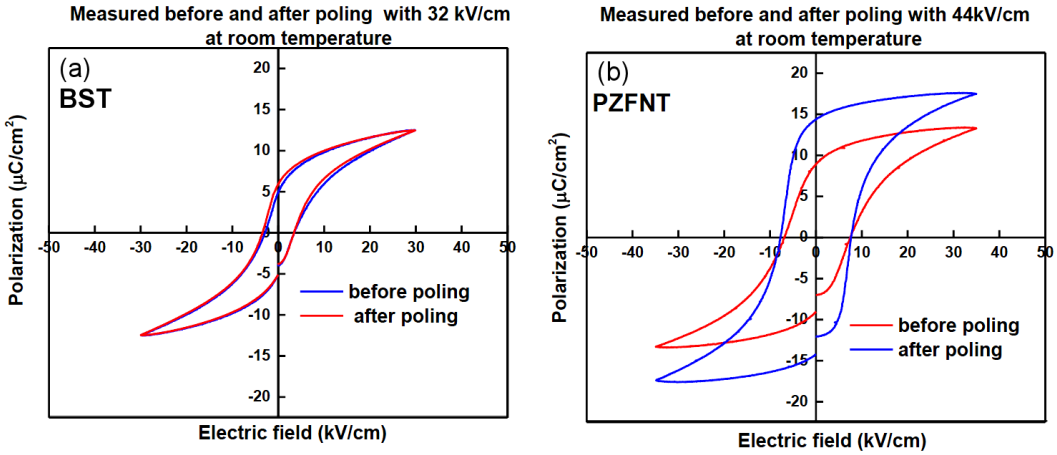

Figure 6. Hysteresis loops measured before and after polling for: a) BST and b) PZFNT ceramics

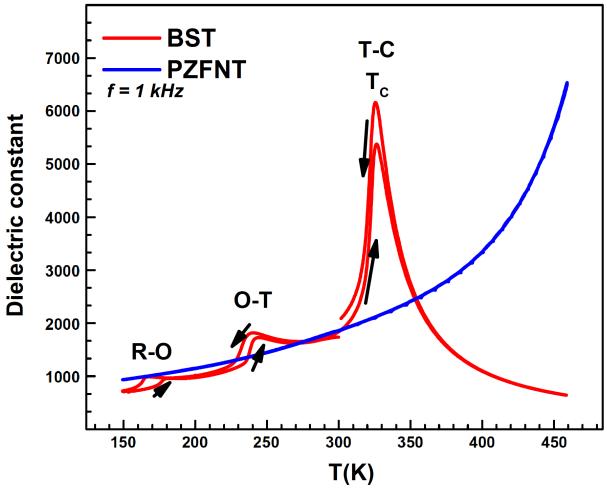

Figure 7. The temperature dependence of the dielectric constant for BST and PZNFT (the dielectric constant was estimated from the capacitance measured at 1 kHz, in vacuum)

Capacitance measurements were registered at 1 kHz in vacuum, on a broad temperature range from −200 °C to 200 °C, in order to determine the dielectric constant and to identify the phase transitions [16]. The temperature dependence of the dielectric constant is represented in Fig. 7 for both materials. The peaks of BST dielectric constant correspond to three phase transitions, two of them between ferroelectric phases at lower temperatures, and the last one between ferroelectric and paraelectric phases, at the higher temperature. PZFNT has no phase transition in this temperature range. Room temperature dielectric constant is 1800 for BST and 1850 for PZFNT.

The temperatures of BST polymorphic transitions between rhombohedral (R), orthorhombic (O), tetragonal (T) and cubic (C) phases and their corresponding dielectric constants are summarized in Table 1. The shift between these temperatures, measured during cooling and heating decreases with increasing temperature, as shown in Fig. 7. Phase transition temperatures and dielectric constants are similar to those reported in the literature [16].

Pyroelectric materials with perovskite structure such as $BaTiO_3$ and $Pb(Zr,Ti)O_3$ (PZT) have been widely used for capacitor and actuator applications near room temperature [19]. For the pyroelectric applications there is only one significant parameter, the value of the total pyroelectric coefficient, defined by the relation [16]:

$$p_t = p + \varepsilon_0 \int_0^E \frac{\partial \varepsilon_s}{\partial T} \mathrm{d}E \qquad (1)$$

The main effect is given by the temperature variation, the second is the deformation of the pyroelectric element and the third represents its thickness in the case of uneven heating. The IR penetration length exceeds the sample thickness at very low frequency and it is comparable to the thickness at higher frequency, so the pyroelectric element can be considered uniformly heated. The induced pyroelectric coefficient (second term) shall be taken into account only in the presence of an electric field applied to the pyroelectric element [16]. The thermal diffusivities (α) of PZT and BST, which have values of $\alpha_{PZT} = 4.1 \cdot 10^{-7}$ m^2/s and $\alpha_{BST} = 10^{-6}$ m^2/s, were considered.

Typical signal of the pyroelectric detector working in the voltage mode can be seen for both samples (Fig. 8), more significant and almost constant at low frequencies, and with decreasing behaviour for high frequencies [20,21].

Table 1. Phase transitions temperatures and dielectric constants for BST ceramics (measurements were performed at 1 kHz)

	R-O		O-T		T-C	
	heating	cooling	heating	cooling	heating	cooling
Temperature [K]	179	165	242	237	326.3	325.6
Dielectric constant	956	986	1728	1816	5380	6160

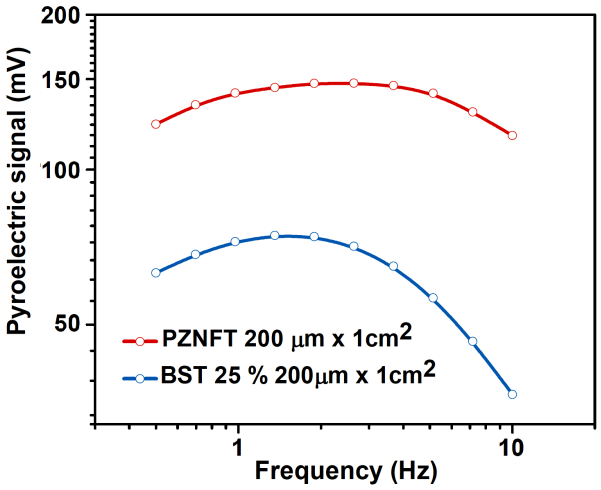

Figure 8. Frequency dependence of the pyroelectric signal

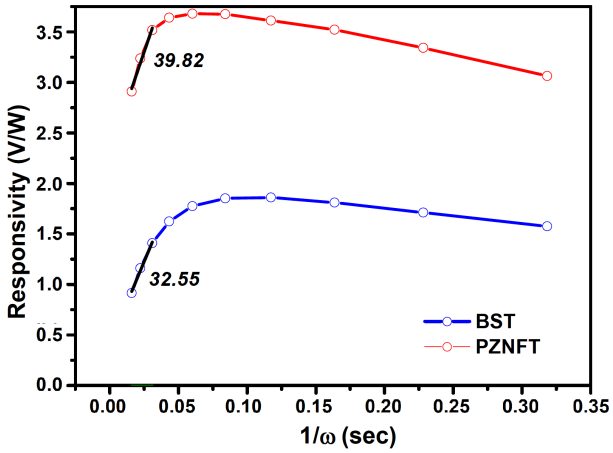

Figure 9. R_V vs. $1/\omega$ representation for PZNFT and BST discs

The pyroelectric signal in the voltage mode of operation has the following dependence on the frequency of the incident radiation [22,23]:

$$S(\omega) = \frac{\omega \cdot \eta \cdot p \cdot A \cdot P_{inc}}{G_T \cdot G_e \cdot (1 + \omega^2 \cdot \tau_T^2)^{1/2} \cdot (1 + \omega^2 \cdot \tau_e^2)^{1/2}} \quad (2)$$

where S is the pyroelectric signal, ω is the pulsation of the IR incident radiation on the pyroelectric element ($\omega = 2\pi f$, with f being the chopping frequency of the IR beam), P^{inc} is the incident power on the active element, η is the emissivity of the electrode exposed to IR radiation, p is the pyroelectric coefficient, A is the area of the sample, G_T is the thermal conductance, G_e is the electric conductance, τ_T is the thermal time constant ($\tau_T = C_T/G_T$, with C_T being the thermal capacity of the pyroelectric element) and τ_e is the electrical time constant ($\tau_e = C_e/G_e$, with C_e being the capacitance of the pyroelectric element). At high frequencies, when both $(\omega \cdot \tau_T)^2$ and $(\omega \cdot \tau_e)^2$ are much larger than unity, $S \approx 1/\omega$ and the previous equation will reduce to [23]:

$$S(\omega) = \frac{\eta \cdot p \cdot A \cdot P_{inc}}{\omega \cdot C_T \cdot C_e} \quad (3)$$

$C_T = \rho \cdot c \cdot A \cdot d$ and $C_e = A \cdot \varepsilon_0 \cdot \varepsilon_r / d$, where ρ is the density, c is the specific heat, ε_0 is the vacuum permittivity, ε_r is the static dielectric constant, and d is the thickness of the ferroelectric ceramics (170 μm for PZT and 250μm for BST).

The voltage responsivity R_V, has a similar dependence on the frequency (Fig. 9) being defined as follows:

$$R_V = \frac{S}{P_{inc}} \quad (4)$$

Using equation (3) in equation (4) and replacing C_T and C_e with above formulas, one can obtain for the voltage responsivity the following relation [20]:

$$R_V = \frac{p}{\varepsilon_0 \cdot \varepsilon_r \cdot \rho \cdot c} \cdot \frac{\eta}{\omega \cdot A} \quad (5)$$

The sample area is $A = 1\ \text{cm}^2$, and the emissivity $\eta 1$ considering that the surface exposed to radiation is covered with black absorber. In this relation, the first part, noted $M = p/\varepsilon_0 \cdot \varepsilon_r \cdot \rho \cdot c$ [24], represents the figure of merit of the material and it can be estimated from the slope of the $R_V = f(1/\omega)$. The following figures of merit were obtained for the two materials: PZT $3.98 \cdot 10^{-3}\ \text{m}^2/\text{C}$ and $3.25 \cdot 10^{-3}\ \text{m}^2/\text{C}$ for BST respectively.

The pyroelectric coefficients for PZNFT and BST ceramics were calculated from the figure of merit, the following values being used for ε_r and ρ_c for PZNFT and BST, respectively: ε_r = 1850; 1800, and ρ_c = $2.6 \cdot 10^6\ \text{J/m}^3\text{K}$; $1.6 \cdot 10^6\ \text{J/m}^3\text{K}$. A two-time larger value was obtained for PZNFT compared to BST: $1.69 \cdot 10^{-4}\ \text{C/m}^2\text{K}$ and $0.82 \cdot 10^{-4}\ \text{C/m}^2\text{K}$. These numbers are comparable or slightly larger than those found in the literature both for BST [25–28] and for PZT [29,30].

IV. Conclusions

$PbZr_{0.68}Fe_{0.14}Nb_{0.14}Ti_{0.04}O_3$ (PZFNT) and $Ba_{0.75}Sr_{0.25}TiO_3$ (BST) ceramics were obtained through the solid-state reaction route. The XRD patterns confirm the presence of a single crystalline phase in both materials. Surface and cross-section SEM images reveal a compact structure with reduced porosity and free of micro-cracks. The uniform distribution of the grain dimensions was beneficial for pyroelectric characterizations. Their dielectric, pyroelectric and ferroelectric properties were determined on very thin ceramic discs of 170 and 250 μm thickness and 30 mm diameter, in order to prove their potential application in laser pulse energy measurement. Both materials have similar room temperature dielectric constants (~2000), but PZFNT shows higher remnant polarization (~15 μ/cm^2) and better pyroelectric properties (~ $1.69 \cdot 10^{-4}$ C/m^{2}K), which recommend it for pyroelectric detectors, for infrared radiation- and for laser pulse energy-meters.

These results represent a step in the development of materials resistant to extreme working conditions, such as laser beam monitoring, radiation and particle detec-

tors. Improving detection performance is a continuous challenge, and can be accomplished by increasing the sensitivity of the devices by integrating the herein investigated elements.

Acknowledgement: The authors acknowledge funding through POC-G project MAT2IT (contract 54/2016, SMIS code 105726, Intermediary Body-Romanian Ministry of Research and Innovation), and the Core Program PN19-03 (contract no. 21 N/08.02.2019).

References

1. A. Lookman, R.M. Bowman, J.M. Gregg, J. Kut, S. Rios, M. Dawber, A. Ruediger, J.F. Scott, "Thickness independence of true phase transition temperatures in barium strontium titanate films", *J. Appl. Phys.*, **96** (2004) 555–562.
2. Y.A. Boikov, T. Claeson, "Degradation of the dielectric permittivity of a strongly oriented $Ba_{0.25}Sr_{0.75}TiO_3$ layer by replacing a $SrRuO_3$ electrode with an Ag one", *Appl. Phys. Lett.*, **80** (2002) 4603–4605.
3. V. Nagarajan, S. Prasertchoung, T. Zhao, H. Zheng, J. Ouyang, R. Ramesh, W. Tian, X.Q. Pan, D.M. Kim, C.B. Eom, H. Kohlstedt, R. Waser, "Size effects in ultrathin epitaxial ferroelectric heterostructures", *Appl. Phys. Lett.*, **84** (2004) 5225–5227.
4. L. Pintilie, I. Boerasu, M.J.M. Gomes, T. Zhao, R. Ramesh, M. Alexe, "Metal-ferroelectric-metal structures with Schottky contacts. II. Analysis of the experimental current-voltage and capacitance-voltage characteristics of $Pb(Zr,Ti)O_3$ thin films", *J. Appl. Phys.*, **98** (2005) 124104.
5. T. Zhang, H. Ni, "Pyroelectric and dielectric properties of sol-gel derived barium–strontium-titanate ($Ba_{0.64}Sr_{0.36}TiO_3$) thin films", *Sens. Actuators Phys.*, **100** (2002) 252–256.
6. F. Fouladi, E. Javid, Y.S. Jalili, "Fabrication and characterization of fast response pyroelectric sensors based on Fe-doped PZT thin films", *J. Mater. Sci. Mater. Electron.*, **27** (2016) 6578–6585.
7. K.W. Kwok, R.C.W. Tsang, H.L.W. Chan, C.L. Choy, "Effects of niobium doping on the piezoelectric properties of sol-gel-derived lead-zirconate–titanate films", *J. Appl. Phys.*, **95** (2004) 1372–1376.
8. O.P. Thakur, J.P. Singh, C. Prakash, P. Kishan, "Modified lead-zirconate-titanate for pyroelectric sensors", *Def. Sci. J.*, **57** (2007) 233–239.
9. Y. Zhang, M. Xie, J. Roscow, Y. Bao, K. Zhou, D. Zhang, C.R. Bowen, "Enhanced pyroelectric and piezoelectric properties of PZT with aligned porosity for energy harvesting applications", *J. Mater. Chem. A*, **5** (2017) 6569–6580.
10. X. Chen, S. Yan, H. Nie, F. Cao, G. Wang, X. Dong, "Improved pyroelectric figures of merit of Mn-doped Zr-rich lead zirconate titanate bulk ceramics near room temperature for energy harvesting applications", *J. Alloys Compd.*, **779** (2019) 450–455.
11. M. Mazzoni, L. Capineri, "A large-area PVDF pyroelectric sensor for CO_2 laser beam alignment", *IEEE Sensors J.*, **7** (2007) 1159–1164.
12. R. Müller, B. Gutschwager, J. Hollandt, M. Kehrt, C. Monte, R. Müller, A. Steiger, "Characterization of a Large-Area Pyroelectric Detector from 300 GHz to 30 THz", *J. Infrared Milli Terahz Waves*, **36** (2015) 654–661.
13. V.R. Mudinepalli, L. Feng, W.-C. Lin, B.S. Murty, "Effect of grain size on dielectric and ferroelectric properties of nanostructured $Ba_{0.8}Sr_{0.2}TiO_3$ ceramics", *J. Adv. Ceram.*, **4** (2015) 46–53.
14. Y. Shi, H. Liu, H. Hao, M. Cao, Z. Yao, Z. Song, G. Li, W. Tang, J. Xie, "Investigation of dielectric properties for $Ba_{0.4}Sr_{0.6}TiO_3$ ceramics with various grain sizes", *Ferroelectrics*, **487** (2015) 109–121.
15. X. Hao, "A review on the dielectric materials for high energy-storage application", *J. Adv. Dielectr.*, **3** (2013) 1330001.
16. J. Ćirković, K. Vojisavljević, N. Nikolić, P. Vulić, Z. Branković, T. Srećković, G. Branković, "Dielectric and ferroelectric properties of BST ceramics obtained by a hydrothermally assisted complex polymerization method", *Ceram. Int.*, **41** [9A] (2015) 11306–11313.
17. A. Young, G. Hilmas, S.C. Zhang, R.W. Schwartz, "Effect of liquid-phase sintering on the breakdown strength of barium titanate", *J. Am. Ceram. Soc.*, **90** (2007) 1504–1510.
18. X. Wang, Y. Zhang, X. Song, Z. Yuan, T. Ma, Q. Zhang, C. Deng, T. Liang, "Glass additive in barium titanate ceramics and its influence on electrical breakdown strength in relation with energy storage properties", *J. Eur. Ceram. Soc.*, **3** (2012) 559–567.
19. A. Ianculescu, I. Pintilie, C.A. Vasilescu, M. Botea, A. Iuga, A. Melinescu, N. Drăgan, L. Pintilie, "Intrinsic pyroelectric properties of thick, coarse grained $Ba_{1-x}Sr_xTiO_3$ ceramics", *Ceram. Int.*, **42** (2016) 10338–10348.
20. B.N. Parida, P.R. Das, R. Padhee, S. Behera, R.N.P. Choudhary, "Structural, dielectric and electrical properties of a new tungsten bronze ferroelectric ceramics", *J. Mater. Sci. Mater. Electron.*, **25** (2014) 2618–2626.
21. D.-S. Kang, M.-S. Han, S.-G. Lee, S.-H. Song, "Dielectric and pyroelectric properties of barium strontium calcium titanate ceramics", *J. Eur. Ceram. Soc.*, **23** (2003) 515–518.
22. D.-S. Paik, S.-E. Park, T.R. Shrout, W. Hackenberger, "Dielectric and piezoelectric properties of perovskite materials at cryogenic temperatures", *J. Mater. Sci.*, **34** (1999) 469–473.
23. R.W. Whatmore, "Pyroelectric devices and materials", *Rep. Prog. Phys.*, **49** (1986) 1335–1386.
24. M. Botea, L. Pintilie, I. Pintilie, V. Stancu, "Indirect amplification of the pyroelectric signal in $Pb(Zr,Ti)O_3$ thin films by the photo-generation of carriers in the Si substrates", *Dig. J. Nanomater. Biostruct.*, **10** (2015) 341–347.
25. M. Botea, A. Iuga, L. Pintilie, "Giant pyroelectric coefficient determined from the frequency dependence of the pyroelectric signal generated by epitaxial $Pb(Zr_{0.2}Ti_{0.8})O_3$ layers grown on single crystal $SrTiO_3$ substrates", *Appl. Phys. Lett.*, **103** (2013) 232902.
26. L. Pintilie, M. Botea, A.Iuga, "Enhancement of pyroelectric signal by continuous ultraviolet illumination of epitaxial $Pb(Zr_{0.2}Ti_{0.8})O_3$ films", *Appl. Phys. Lett.*, **105** (2014) 132901.
27. L. Pintilie, C. Constantin, "Dielectric and pyroelectric properties of a ceramic bimorph structure", *Ferroelectrics*, **173** (1995) 111–124.
28. J.H. Yoo, W. Gao, K.H. Yoon, "Pyroelectric and dielectric bolometer properties of Sr modified $BaTiO_3$ ceramics", *J. Mater. Sci.*, **34** (1999) 5361–5369.
29. H.M. Jang, Y.H. Jun, "$(Ba,Sr)TiO_3$ system under DC-bias field: II. Induced and intrinsic pyroelectric coefficients and figures-of-merit", *Ferroelectrics*, **193** (1997) 125–140.

30. J. Lee, J.-S. Park, J.-S. Kim, J.-H. Lee, Y. Lee, S.-R. Hahn, "Preparation of (Ba,Sr)TiO_3 thin films with high pyroelectric coefficients at ambient temperatures", *Jpn. J. Appl. Phys.*, **38** (1999) L574–L576.
31. J.-G. Cheng, J. Tang, X.-J. Meng, S.-L. Guo, J.-H. Chu, M. Wang, H. Wang, Z. Wang, "Fabrication and Characterization of pyroelectric $Ba_{0.8}Sr_{0.2}TiO_3$ thin films by a sol-gel process", *J. Am. Ceram. Soc.*, **84** (2001) 1421–1424.
32. L. Pintilie, I. Pintilie, I. Matei, "Equivalent pyroelectric coefficient of a pyroelectric bimorph structure", *J. Appl. Phys.*, **88** (2000) 7264–7271.
33. V. Stancu, L. Amarande, M. Botea, M. Cioangher, A.G. Tomulescu, A. Iuga, L. Pintilie , "Structural, dielectric and pyroelectric properties of Nb and Fe doped PZT ceramics", *Dig. J. Nanomater. Biostructures*, **14** (2019), 225–230.